Multivalent mannose-displaying nanoparticles constructed from poly{styrene-*co*-[(maleic anhydride)-*alt*-styrene]}†

Rongmin Su,[a] Lei Li,[b] Xiaoping Chen,[a] Jiahuai Han[c] and Shoufa Han*[a]

Received 10th October 2008, Accepted 4th December 2008
First published as an Advance Article on the web 17th March 2009
DOI: 10.1039/b817823b

Micellar mannose nanoparticles were constructed from poly{styrene-*co*-[(maleic anhydride)-*alt*-styrene]} with fluorophores or quenchers doped into the hydrophobic inner cores, allowing the direct monitoring of multivalent lectin–glycan interactions. The mannose-displaying nanoparticles bind Con A and sperm surface lectins with high affinity, suggesting their broad utility for modulating protein–carbohydrate interaction mediated cell surface biology.

Introduction

Cell surface protein–glycan interactions mediate a variety of biological processes ranging from viral infections, cancer cell metastasis, to cell signaling events, *etc.*[1] Lectins, which are glycan-binding proteins, typically bind their monovalent ligands with low affinity. Although the intrinsic affinities of lectin–glycan interactions are low, nature utilizes multivalency to achieve stable binding for the initiation of subsequent biological activities.[1] For instance influenza virus, with k_d values at mM levels towards monomeric sialoside ligands,[2] binds cell surface sialosides in a polyvalent manner with avidity that leads to effective viral infections. Probes capable of inhibiting cell surface lectin–glycan interactions have potential therapeutic applications in combating viral infections, and cancer metastasis, *etc.*[3–5] Currently, the design of ligand-based probes of lectins largely relies on the display of multivalent glycan ligands on selected scaffolds including polymers, dendrimers, nanoparticles, virus, *etc.*[6–11] Some of these systems suffer from multistep syntheses, low overall yields, moderately enhanced lectin binding affinity, or a lack of facile methods for direct characterization of probe–lectin interactions.

Hairy micellar nanoparticles, with coronas comprised of hydrophilic linear polymers and hydrophobic cores, can be assembled from amphiphilic diblock copolymers in aqueous solutions. We envisioned that the incorporation of glycan ligands onto hydrophilic polymer chains located at the corona could lead to novel glyco-probes that combine the advantages of both linear polymers and nanoparticles. In hairy glyco-nanoparticles, the flexibility of the polymer chains together with the tunable size of the nanoparticles will allow simultaneous binding of the hairy nanoparticle surface glycans with multimeric lectins or multiple lectin molecules on host cell surfaces. The efficient multivalent glycan–lectin interaction is essential for enhanced binding affinity. Furthermore, the hydrophobic inner cores of micellar nanoparticles have been utilized to entrap hydrophobic drugs.[12] Similarly, hydrophobic fluorophores can be doped into the hydrophobic cores, which facilitates the monitoring of lectin–glycan interactions.

Poly{styrene-*co*-[(maleic acid)-*alt*-styrene]}, a well-known amphiphilic diblock copolymer capable of forming micellar nanoparticles in aqueous solutions, was employed as the scaffold to display mannose. Mannose–lectin interactions are vital in a broad spectrum of physiological processes including human fertilization,[13] and pathogen–host cell recognition.[14,15] Hence, mannose is used as a model ligand to incorporate into poly{styrene-*co*-[(maleic anhydride)-*alt*-styrene]} for evaluation of the efficacy of the new scaffold in multivalent lectin–glycan interactions.

Results and discussion

Low affinity cell surface glycan receptors that function through multivalent interactions are intrinsically poor targets for the rational design of ligands that will bind to the cell. The molecular size of a lectin is generally about several nanometers. The spacing between glycan ligands displayed on traditional scaffolds, like symmetrical dendrimers, is too small to bridge lectin subunits or multiple lectins on the cell surface. The flexible hydrophilic chains radiating from size-tunable hydrophobic cores render hairy micellar glyco-nanoparticles constructed from poly{styrene-*co*-[(maleic acid)-*alt*-styrene]} suitable for simultaneous binding with a large number of lectins on cell surfaces. Additional advantageous features of poly{styrene-*co*-[(maleic acid)-*alt*-styrene]} as glycan-displaying scaffolds include: (1) the anhydride moieties on the poly(maleic anhydride-*alt*-styrene) fragment can be easily amidated by amine-containing glycan ligands in high yields; (2) the number and density of glycan ligands on the nanoparticle surface can be controlled by variation of the degree of polymerization of the poly(maleic anhydride-*alt*-styrene) fragment; (3) amphiphilic diblock copolymers self-assemble in water and form nanoparticles with hydrophobic cores that can trap fluorescence quenchers or fluorophores for direct monitoring of lectin–glycan probe interactions or cell surface labeling.

Poly{styrene-*co*-[(D-mannopyranosyl-α-1-ethylamidomaleic acid)-*alt*-styrene] was successfully prepared by amidation of poly{styrene-*co*-[(maleic anhydride)-*alt*-styrene]} with α-1-O-(2′-aminoethyl)-D-mannopyranoside (compound **1**) (Scheme 1). As compared with that of the non-glycosylated polymer

[a]*Department of Chemistry, College of Chemistry and Chemical Engineering, and The Key Laboratory for Chemical Biology of Fujian Province, Xiamen University, 361005, P. R. China. E-mail: shoufa@xmu.edu.cn*
[b]*College of Materials, Xiamen University, 361005, P. R. China*
[c]*College of Life Science, Xiamen University, 361005, P. R. China*
† Electronic supplementary information (ESI) available: Further experimental methods and results. See DOI: 10.1039/b817823b

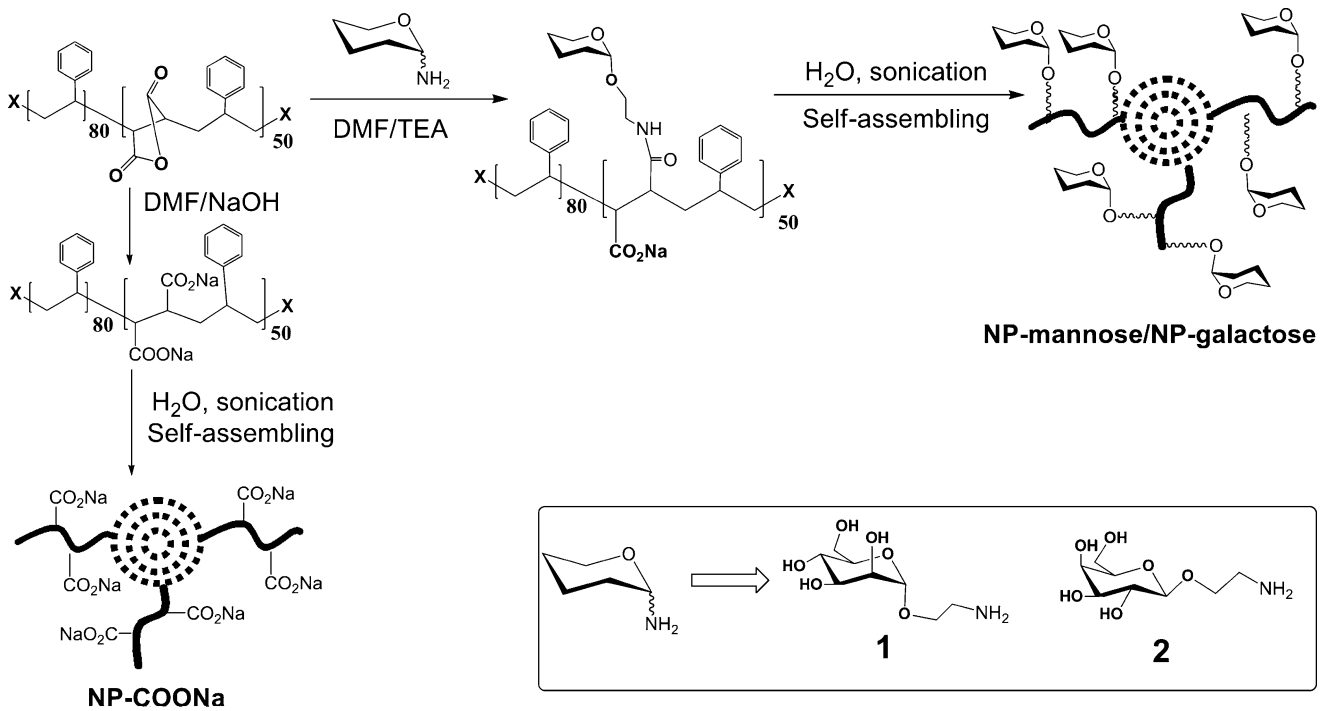

Scheme 1 Synthesis and assembling of hairy glyco-nanoparticles from poly{styrene-*co*-[(maleic anhydride)-*alt*-styrene]}.

(NP-COONa) (Figure 6S, ESI†), the ^{1}H-NMR spectrum of the NP-mannose showed extra signals (*e.g.* δ 4.5) which originated from incorporated mannose (Figure 5S, ESI†). The exact amount of mannose incorporated in the polymer, titrated using a reported colorimetric assay,[16] was 350 μg per mg of polymer (Table 1S, ESI†), suggesting that the anhydride moiety was amidated in roughly quantitative yield. Assembly of the resultant mannosylated polymer together with 2-{[4-(dimethylamino)phenyl]azo}-benzoic acid, ethyl ester (ethyl ester of methyl red, fluorescence quencher) or rhodamine 6G (fluorophore) afforded hairy nanoparticles with mannose on the surface (designated as NP-mannose) doped with fluorescence quencher or fluorophores. The statistical mean diameter size of NP-mannose was 89.3 nm as determined by dynamic light scattering (Fig. 1).

Generally, the size of a protein molecule is in the range of several nanometers. Thus, more than one order of magnitude of difference in the diameters of NP-mannose relative to lectin molecules renders NP-mannose spatially accessible to multimeric lectin molecules or a large number of lectins on cell surfaces simultaneously. To evaluate the efficacy of the hairy nanoparticles as multivalent glycan probes, the interaction of NP-mannose with concanavalin-A (Con A) was investigated. Con A lectin from Jack bean exists as a homotetramer at physiological conditions. Each monomeric subunit of Con A has one binding site for D-mannose. Con A has been used extensively as a model lectin to evaluate the efficacy of various scaffolds displaying multivalent mannose, mainly *via* hemagglutination assays.[9] Although hemagglutination assays have been frequently used to give the relative activity of various glyco-probes by their inhibition of lectin induced red blood cell agglutination, they do not provide information regarding binding affinity.[9] In contrast, in our system lectin–glycan interactions could be directly monitored *via* fluorescence resonance energy transfer (FRET) between the fluorescein isothiocyanate-labeled Con A (FITC-Con A) (donor) with the ethyl ester of methyl red trapped in the NP-mannose cores (quencher) (Scheme 2). Correlation of the fluorescence signals of the glyco-probes with added inhibitory

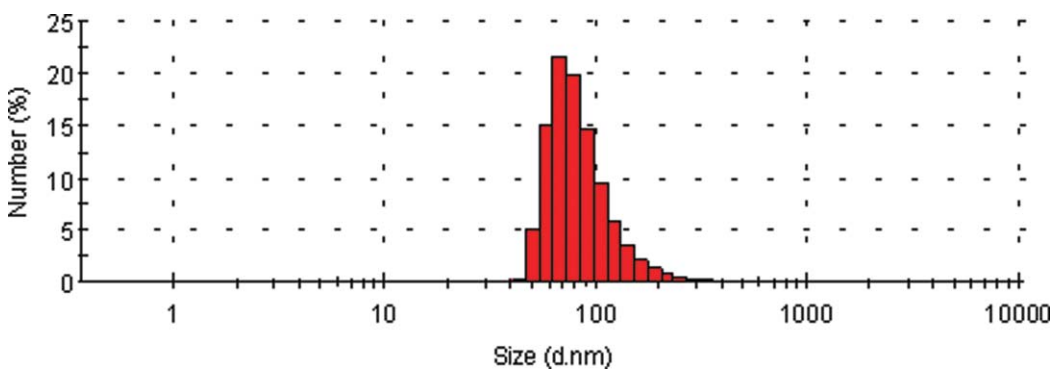

Fig. 1 Diameter size of NP-mannose measured by dynamic light scattering. The statistical mean size of NP-mannose was 86.9 nm.

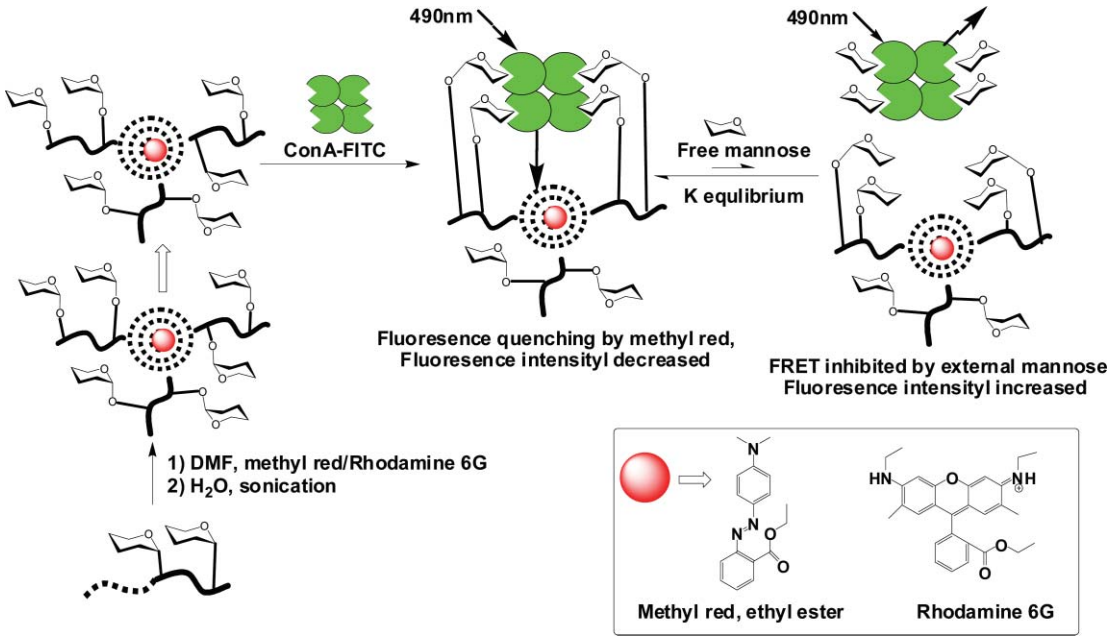

Scheme 2 Theoretical representation of FRET based competitive binding assay between FITC-Con A and NP-mannose with trapped methyl red in the presence of D-mannose.

species allows direct evaluation of their relative binding affinity to a lectin. The new assay is simple and straightforward, offering a valuable alternative to currently employed hemagglutination assays in the study of protein–glycan interaction.

The fluorescence intensity of FITC-Con A was greatly suppressed in the presence of NP-mannose owing to quenching of the fluorescence by methyl red (Fig. 2, **A**). In an analogous experiment, no obvious FRET was observed between FITC-Con A and NP-galactose with ethyl ester of methyl red doped in the hydrophobic cores (Scheme 1) (Figure 10S, ESI†). The dfference in FRET efficiency between NP-mannose and NP-galactose in the presence of FITC-Con A indicates that the formation of FITC-Con A/NP-mannose complexes was mannose dependent. To probe the multivalent effects between NP-mannose and tetrameric Con A, D-mannose monosaccharide was added to the FITC-Con A/NP-mannose complex at various concentrations. The fluorescence emission spectra, recorded as a function of the concentration of D-mannose (Fig. 2, **A**), showed that fluorescence intensity of the FITC-Con A/NP-mannose complex increased with addition of D-mannose. The FRET efficiency of the donor–quencher pair was distance-dependant. Thus in the presence of free mannose that competed with NP-mannose for the lectinic binding sites, Con A was stripped off the NP-mannose leading to enhanced detectable fluorescence (Scheme 2). The recovery of fluorescence relative to free FITC-Con A was about 20% in presence of 1.5M of D-mannose (Figure 10S, ESI†). In the control experiments, the fluorescence of FITC-Con A was not obviously affected by the mannose monosaccharide at concentrations employed in the inhibitory assays. Based on the inhibitory FRET studies, the half maximal inhibition concentration (IC_{50}) of mannose on the formation of NP-mannose/Con A complex was about 1.5M. Based on the reported colorimetric assay,[16] the concentration of the nanoparticle-bound mannose in the assay conditions was determined to be 3 μM. The binding equilibrium, calculated using the equation K_{eq} = [mannose/Con A][NP-mannose]/[NP-mannose/Con A][mannose] (Scheme 2), favored the formation of the NP-mannose/Con A complex by roughly 5 orders of magnitude relative to the D-mannose/Con A complex, indicating that multivalent binding to the tetrameric subunits of Con A was occurring (Scheme 2). The FRET between fluorescently labeled lectins and the dye-doped glyco-nanoparticles allows spectrofluorimetric monitoring of the protein–glycan interactions, offering a facile method of directly comparing the relative binding affinity of different glyco-probes towards selected lectins.

To verify the hypothesis that the affinity between NP-mannose and tetrameric Con A was due to simultaneous binding of the four ligand binding sites by mannose on the nanoparticle surface, we sought to study the interaction of NP-mannose with dimeric Con A. Con A dissociates into dimers at pH 6.5 or below.[17] The FRET based competitive binding assay was performed in sodium acetate buffer (50 mM, pH 5.5). The emission spectra of the solutions are shown in Fig. 2 (**B**). The inhibition efficiency of the binding of NP-mannose with dimeric FITC-Con A to the concentrations of exogenous mannose was much more sensitive than was the binding to tetrameric Con A. The recovery of fluorescence reached 30% in the presence of 0.1M of D-mannose, indicating that the binding affinity between dimeric Con A and the mannose-nanoparticles was at least 150 times weaker than compared with tetrameric Con A. The observed significant differences in affinity on the basis of Con A valency are supportive of multiple binding with ligand binding sites by NP-mannose.

Mannose-binding lectin expressed on sperm cell surfaces is vital for sperm–oocyte fusion.[18–20] Demonstrated to bind Con A with high affinity, NP-mannose was further tested for its ability to bind cell surface lectins. NP-COONa, the control assembled from polystyrene-*co*-poly(maleic acid, sodium salt-*alt*-styrene) (Scheme 1), and NP-mannose with rhodamine 6G trapped in the hydrophobic cores (Scheme 2) were separately incubated with

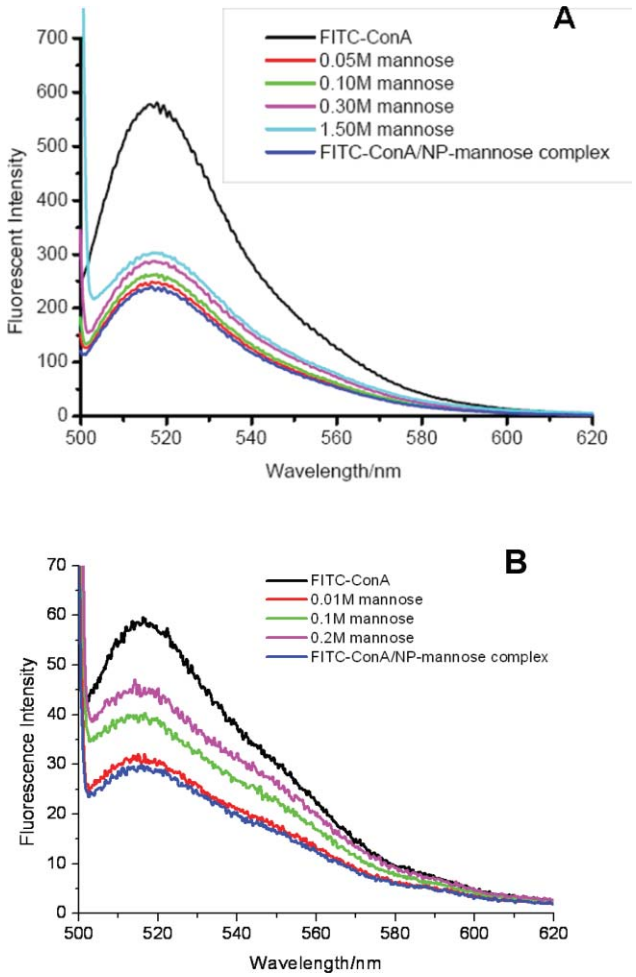

Fig. 2 Inhibitory effects of D-mannose on the fluorescence emission of tetrameric FITC-Con A doped with methyl red (0.13 μg/mL) (**A**) and dimeric FITC-Con A doped with methyl red (0.13 μg/mL) (**B**) in the presence of NP-mannose (0.13 μg/mL).

semen specimens in PBS buffer. Fluorescence microscopy revealed normal morphology for the sperms treated with NP-COONa. The fluorescence on the cell surface is probably due to ionic interactions between sperms and polyanionic compounds.[21] In the presence of multivalent NP-mannose, the sperm cells tend to aggregate as compared with sperms incubated with NP-COONa (Fig. 3) presumably due to the binding of NP-mannose with multiple lectin molecules on neighboring sperms. The cell morphology of NP-mannose treated sperms was altered and no sperms with normal heads and tails could be identified probably due to interference by NP-mannose binding on cell surface lectins. Investigation of the interference of free mannose monosaccharide on the interaction of NP-mannose with sperms was also performed using the same procedure with the addition of various amounts of mannose. The aggregation of sperms was gradually inhibited with increasing amounts of mannose. At high concentrations of mannose (2M), normal morphology of sperms was observed (Figure 12S, ESI†). The inhibitory effects of high concentrations of mannose indicate that the interaction between NP-mannose and sperm cell surface lectins is much stronger than with monovalent mannose. D-mannose derivatives and D-mannose monosaccharide have been documented to block fertilization.[19,13,22] Multivalent mannose probes that could bind sperm with higher affinity might be superior fertilization inhibitors than mannose monosaccharide. Our preliminary results suggest that it is worth evaluating the inhibition efficacy of NP-mannnose on sperm–oocyte fusion for potential utility as novel topical contraceptive reagents.

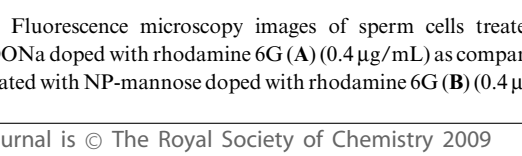

Fig. 3 Fluorescence microscopy images of sperm cells treated with NP-COONa doped with rhodamine 6G (**A**) (0.4 μg/mL) as compared with cells treated with NP-mannose doped with rhodamine 6G (**B**) (0.4 μg/mL).

Conclusions

Mannose displaying hairy nanoparticles were easily assembled from polystyrene-*co*-poly(maleic anhydride-*alt*-styrene) and bound lectins in a multivalent manner. Due to the high lectin binding affinity and other advantageous features mentioned above, hairy micellar glyco-nanoparticles have broad application in the study of protein–glycan interactions.

Experimental

Materials and methods

α-1-O-(2′-Aminoethyl)-D-mannopyranoside (**1**) and β-1-O-(2′-aminoethyl)-D-galactopyranoside (**2**) (Scheme 1) were synthesized according to the reported literature.[23] Poly{styrene-*co*-[(maleic anhydride)-*alt*-styrene]} was prepared following a published procedure.[24] Unless otherwise noted, all reagents or lectins were obtained commercially from either Alpha-Aesar or Sigma-Aldrich and used without further purification. Column chromatography was performed on silica gel (300–400 mesh). NMR spectra (^{1}H at 400 MHz and ^{13}C at 100 MHz) were recorded on a Bruker instrument using tetramethyl silane as the internal reference. The fluorescence emissions were performed on a spectrofluorimeter (Shimadzu, RF-5301, Japan) using the excitation wavelength (λex) of 490 nm. The fluorescence microscopy of sperms was visualized and recorded using a phase-contrast microscope (Olympus, Japan) (×100 magnification). Dynamic light scattering experiments were performed on Malvern Nano-ZS & MPT-2 (U.K.).

Synthesis of 2-{[4-(dimethylamino)phenyl]azo}-benzoic acid, ethyl ester (ethyl ester of methyl red)

To a 25 mL flask containing dry ethanol (10 mL) was added 4-dimethylaminopyridine (DMAP, 4.8 mg, 0.04 mmol), 1-ethyl-3-(3-dimethylaminopropyl)carbodiimide hydrochloride (EDC, 1.0 g, 5 mmol) and 2-{[4-(dimethylamino)phenyl]azo}-benzoic acid (methyl red, 0.59 g, 2 mmol) (Scheme 1S, ESI†). The reaction mixture was stirred at room temperature overnight. The reaction was monitored by TLC. When the reaction was complete, the solvent was removed by rotary evaporation and the resulting residue was

suspended in dichloromethane (30 ml). The organic solution was washed with aqueous hydrochloric acid (1M, 20 ml), dried with Na_2SO_4, filtered, and concentrated by rotary evaporation. The crude product was further purified by column chromatography over silica gel to afford the desired product as an orange solid (0.5 g) in 76% yield. $R_f = 0.5$ (1:5, ethyl acetate/petroleum ether); ^{1}H-NMR ($CDCl_3$): δ 1.31 (t, 3H, J = 7.16 Hz), 3.10 (s, 6H), 4.36 (q, 2H, J = 7.13 Hz), 6.74 (d, 2H, J = 9.11 Hz), 7.40 (t, 1H, J = 6.42 Hz), 7.55 (t, 1H, J = 6.42 Hz), 7.62 (d, 1H, J = 7.07 Hz), 7.77 (d,1H, J = 6.46 Hz), 7.87 (d, 2H, J= 5.19 Hz) (Figure 3S, ESI†); ^{13}C-NMR ($CDCl_3$): 14.37, 40.26, 61.18, 111.38, 119.11, 125.39, 128.22, 128.36, 129.47, 131.57, 143.73, 152.46, 152.65, 168.32 (Figure 4S, ESI†); MS (ESI, $C_{17}H_{19}N_3O_2$): calculated [MH^+]: 298.2, found: 298.2.

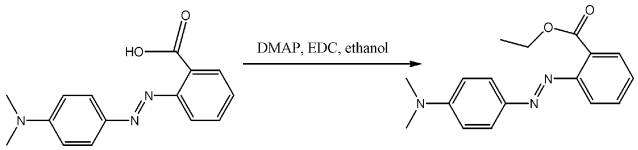

Preparation of NP-mannose hairy nanoparticles doped with the ethyl ester of methyl red or rhodamine 6G

α-1-O-(2′-Aminoethyl)-D-mannopyranoside (30 mg), triethylamine (0.1 mL) and poly{styrene-*co*-[(maleic anhydride)-*alt*-styrene]} (20 mg) were added to a 5 ml flask containing DMF (1 mL). The solution was stirred at ambient temperature overnight followed by addition of ethyl ester of methyl red (1 mg) or rhodamine 6G (1 mg) and then water (15 mL). The resultant mixture was extensively dialyzed against deionized water using a dialysis tube (MWCO 3000) to remove excess compound **1**, DMF, and triethylamine, and then was sonicated for 40 minutes to afford a clear solution. The solution was filtered through a 0.22 μm filter to give poly{styrene-*co*-[(D-mannopyranosyl-α-1-ethylamidomaleic acid)-*alt*-styrene]} nanoparticles (designated as NP-mannose) (Scheme 1) doped with ethyl ester of methyl red or rhodamine 6G. The statistical mean diameter size of NP-mannose was 89.3 nm as determined by dynamic light scattering.

Preparation of NP-galactose hairy nanoparticles doped with the ethyl ester of methyl red

β-1-O-(2′-Aminoethyl)-D-galactopyranoside (30 mg), triethylamine (0.1 mL) and poly{styrene-*co*-[(maleic anhydride)-*alt*-styrene]} (20 mg) were added to a 5 ml flask containing DMF (1 mL). The solution was stirred at ambient temperature overnight followed by addition of ethyl ester of methyl red (1 mg) and then water (9 mL). The mixture was first extensively dialyzed against deionized water using a dialysis tube (MWCO 3000) to remove excess compound **2**, DMF, and triethylamine and then ultrasonicated for 20 minutes affording poly{styrene-*co*-[(D-galactopyranosyl-β-1-ethylamidomaleic acid)-*alt*-styrene]} nanoparticles (NP-galactose) (Scheme 1) doped with ethyl ester of methyl red. The statistical mean diameter size of NP-galactose was 26 nm as determined by dynamic light scattering (Figure 9S, ESI†).

Preparation of NP-COONa nanoparticles doped with rhodamine 6G

Aqueous NaOH solution (1M, 0.3 mL) was added to a 5 ml flask containing DMF (1 mL) and poly{styrene-*co*-[(maleic anhydride)-*alt*-styrene]} (20 mg). The solution was stirred at ambient temperature for 4 hours. To the stirred solution was added rhodamine 6G (1 mg) and then water (9 mL). The solution was neutralized with hydrochloric acid (1M) to pH 7.0, ultrasonicated for 20 minutes, and then extensively dialyzed against deionized water using a dialysis tube (MWCO 3000), affording poly{styrene-*co*-[(maleic acid, sodium salt)-*alt*-styrene]} nanoparticles (designated as NP-COOH) (Scheme 1) doped with rhodamine 6G. The statistical mean diameter size of NP-COONa was 35.2 as determined by dynamic light scattering.[25]

FRET based competitive binding assays of tetrameric FITC-Con A/NP-mannose complex

Tetrameric FITC-Con A/NP-mannose complex was formed *via* incubation of solutions containing mannose-NP (0.4 μg), FITC-labeled Con A (0.4 μg) in Tris-HCl buffer (50 mM, pH 7.2, 50 μL) containing calcium chloride (2 mM) (buffer A) and manganese chloride (2 mM) at room temperature for 15 minutes. Then various volumes of D-mannose solution in buffer A (3M) and tetrameric FITC-Con A/NP-mannose complex solution (50 μL) were added to cuvettes. The final volume was adjusted to 3 mL with addition of Buffer A. The fluorescence emission spectra were recorded as a function of the concentrations of D-mannose monosaccharide.

FRET based competitive binding assays of dimeric FITC-Con A/NP-mannose complex

Dimeric FITC-Con A/NP-mannose complex was formed *via* incubation of solutions containing NP–mannose (0.4 μg), FITC-labeled Con A (0.4 μg) in sodium-acetate buffer (50 mM, pH 5.5, 50 μL) containing calcium chloride (2 mM) and manganese chloride (2 mM) (buffer B) at room temperature for 15 minutes. Then various volume of D-mannose solution in buffer B (3M) and dimeric FITC-Con A/NP-mannose complex solution were added to cuvettes containing buffer B for 20 minutes. The final volume was adjusted to 3 mL with addition of buffer B. The fluorescence emission spectra were recorded as a function of the concentrations of D-mannose monosaccharide.

Binding of NP-mannose with human spermatozoa

Human spermatozoa samples were stained using the procedure described in the published literature.[18] Briefly, NP-mannose (0.4 μg/mL) and NP-COONa (0.4 μg/mL) doped with rodamine 6G were separately incubated with human spermatozoa for 20 min at 37 °C in HEPES buffer (30 mM, pH 7.0) containing NaCl (150 mM), $MgCl_2$ (0.5 mM), $CaCl_2$ (20 mM) and bovine serum albumin (1%, w/v). Spermatozoa were then washed three times with HEPES buffer without calcium chloride, pipetted onto glass slides and fixed on cover glass. The morphology of the sperm cells was visualized using a phase-contrast microscope.

Acknowledgements

This work was supported by Chinese 863 project (No. 2006AA02Z164) and National Natural Science Foundation of China (No. 20842001 and 20802060).

References

1 B. E. Collins and J. C. Paulson, *Curr. Opin. Chem. Biol.*, 2004, **8**, 617–25.
2 J. E. Hanson, N. K. Sauter, J. J. Skehel and D. C. Wiley, *Virology*, 1992, **189**, 525–33.
3 J. Rojo, V. Diaz, J. M. de la Fuente, I. Segura, A. G. Barrientos, H. H. Riese, A. Bernad and S. Penades, *ChemBioChem*, 2004, **5**, 291–7.
4 R. Stahn and R. Zeisig, *Tumour Biol.*, 2000, **21**, 176–86.
5 W. J. Lees, A. Spaltenstein, J. E. Kingery-Wood and G. M. Whitesides, *J. Med. Chem.*, 1994, **37**, 3419–33.
6 E. Kaltgrad, M. K. O'Reilly, L. Liao, S. Han, J. C. Paulson and M. G. Finn, *J. Am. Chem. Soc.*, 2008, **130**, 4578–9.
7 N. Sharon and H. Lis, *Sci. Am*, .1993, **268**, 82–9.
8 L. L. Kiessling, J. E. Gestwicki and L. E. Strong, *Curr. Opin. Chem. Biol.*, 2000, **4**, 696–703.
9 E. K. Woller and M. J. Cloninger, *Org Lett*, .2002, **4**, 7–10.
10 Z. Dai, A. N. Kawde, Y. Xiang, J. T. La Belle, J. Gerlach, V. P. Bhavanandan, L. Joshi and J. Wang, *J. Am. Chem. Soc.*, 2006, **128**, 10018–9.
11 A. Robinson, J. M. Fang, P. T. Chou, K. W. Liao, R. M. Chu and S. J. Lee, *ChemBioChem*, 2005, **6**, 1899–905.
12 L. Y. Qiu and Y. H. Bae, *Pharm. Res.*, 2006, **23**, 1–30.
13 K. Mori, T. Daitoh, M. Irahara, M. Kamada and T. Aono, *Am. J. Obstet. Gynecol.*, 1989, **161**, 207–11.
14 L. Heggelund, T. E. Mollnes, T. Ueland, B. Christophersen, P. Aukrust and S. S. Froland, *J. Acquir. Immune Defic. Syndr.*, 2003, **32**, 354–61.
15 I. Ofek, A. Mosek and N. Sharon, *Infect. Immun.*, 1981, **34**, 708–11.
16 M. G. K. A. Dubois, J. K. Hamilton, P. A. Rebers and F. Smith, *Anal. Chem.*, 1956, **28**, 350–356.
17 T. W. Hamelryck, J. G. Moore, M. J. Chrispeels, R. Loris and L. Wyns, *J. Mol. Biol.*, 2000, **299**, 875–83.
18 A. Gabriele, G. D'Andrea, G. Cordeschi, G. Properzi, M. Giammatteo, C. De Stefano, R. Romano, F. Francavilla and S. Francavilla, *Mol. Hum. Reprod.*, 1998, **4**, 543–53.
19 S. Tanghe, A. Van Soom, L. Duchateau and A. De Kruif, *Mol. Reprod. Dev.*, 2004, **67**, 224–32.
20 H. M. Youssef, G. F. Doncel, B. A. Bassiouni and A. A. Acosta, *Fertil. Steril.*, 1996, **66**, 640–5.
21 E. Howes, J. C. Pascall, W. Engel and R. Jones, *J. Cell. Sci.*, 2001, **114**, 4127–36.
22 K. Mori, T. Daitoh, M. Kamada, N. Maeda, M. Maegawa, K. Hirano, M. Irahara and T. Aono, *Hum. Reprod.*, 1993, **8**, 1729–32.
23 T. Hasegawa, T. Fujisawa, M. Numata, T. Matsumoto, M. Umeda, R. Karinaga, M. Mizu, K. Koumoto, T. Kimura, S. Okumura, K. Sakurai and S. Shinkai, *Org. Biomol. Chem.*, 2004, **2**, 3091–8.
24 M. Q. Zhu, L. H. Wei, M. Li, L. Jiang, F. S. Du, Z. C. LI and F. M. Li, *Chem. Commun.*, 2001, 365–366.
25 W. Fang *et al.*, *Bioorg. Med. Chem. Lett.*, 2009, DOI: 10.1016/j.bmcl.2009.02.059.